Gap independent coupling into parallel plate terahertz waveguides using cylindrical horn antennas

Alisha J. Shutler and D. Grischkowsky[a)]
School of Electrical and Computer Engineering, Oklahoma State University, Stillwater, Oklahoma 74078, USA

We demonstrate how replacing the silicon lenses, traditionally used to couple radiation into parallel plate waveguides, with integrated cylinder-based horn couplers not only greatly improves ease of use and fabrication but also features gap independent coupling. The couplers, created from chords of a cylinder, give reflection free transmission through the waveguide that is on the order of the quasi-optical approach. The gap independent coupling is demonstrated through a precise measurement of the metal conductivity of the THz skin depth layer. © 2012 American Institute of Physics. [http://dx.doi.org/10.1063/1.4754846]

I. INTRODUCTION

Since its introduction into the THz community,[1] the parallel plate waveguide has contributed to the enhancement of a number of applications, including high resolution spectroscopy,[2–4] sensing,[5,6] imaging,[7] and guiding,[8] in large part due to its ability to propagate the TEM mode polarized THz signal with nearly dispersion free and low-loss transmission. The Fresnel losses introduced by the typically used silicon lens based method of coupling the THz radiation into the waveguide account for up to 50% in total transmission losses; the coupling to the waveguide, independent of waveguide absorption, reduces the total transmission to 32%.[9] Previous work suggested that the relatively large waveguide absorption losses were largely dependent upon the reduced conductivity of the skin depth layer which occurred because of surface and lattice defects.[10] Because the nature of the silicon lenses only allows a fixed and limited amount of THz signal compression into the sub-wavelength confinement of the guide, measuring the conductivity of the parallel plates has proven to be challenging, as the coupling does not remain constant when the plate separation is changed. Since absorption, and consequently, conductivity measurements are based on the waveguide assembly's ability to couple in radiation, inconsistent coupling can produce erroneous results. Here, we introduce a new type of parallel-plate waveguide with an integrated coupling scheme to simultaneously remove Fresnel losses, reflections, and to provide a constant coupling of the THz wave, independent of gap size between the parallel plates.

II. DESIGN

The new waveguides are based on the adiabatic compression of a THz wave[11] by using a pair of chords from a cylinder as the integral coupling device.[12] Similar devices have previously been developed,[13] but our design benefits from the straightforward use of simple chords to produce a device of comparable performance to the commonly used quasi-optics approach. The parallel plates can be introduced directly onto the chords by milling out a flat on the middle section of the chords, creating an integrated parallel plate waveguide (CYLWG). Larger radius cylinders yield longer sections of chord, and a smoother, more adiabatic transmission onto the parallel surfaces. Using this concept, we made two types of identical waveguides, one out of aluminum alloy and the other out of copper, using 8 in. (20.32 cm) radius-of-curvature chords. The dimensions of the waveguide are given in Fig. 1. For each waveguide, two opposing plates were created, one with countersunk holes for 4/40 mounting screws and the other with threaded holes at the indicated positions in Fig. 1. Plate spacings, or gaps, between the waveguides were determined by small strips of metal shims varying in thickness from $12.5\,\mu m$ to $200\,\mu m$, placed onto the waveguide's flat region, just outside of the THz beam extent. These metal strips were cut to fit within the $6.15 \times 30\,mm$ space (indicated in grey) around the threaded screw holes, and were hole punched in order to allow passage of the tightening screws. The assembled waveguide was then placed into the confocal beam waist of a standard THz-TDS system, as seen in Fig. 1, aligning the center of the parallel plates with the center of the beam-waist.

The THz-TDS system uses two photoconductive switches to generate and detect THz radiation. The switches are driven by a pulse train from an 800 nm, 100 fs, 80 MHz mode-locked Ti-sapphire femtosecond laser. The emitted THz radiation is collimated by a high-resistivity silicon lens onto a 90° parabolic mirror with a 12.5 cm focal length. Another parabolic mirror, located 25 cm downstream at twice the focal distance from the first, directs the radiation onto a second high-resistivity silicon lens and onto the receiver, creating what is known as a 4f system. The entire system is located in an airtight enclosure to overcome the effects of atmospheric water vapor absorption on the THz beams. The system can achieve a time domain signal-to-noise ratio of 10 000:1.

III. EXPERIMENT

The waveguides were placed symmetrically at the center of the beam-waist in the THz-TDS system, and THz pulses transmitted through the waveguide were measured, with

a)Author to whom correspondence should be addressed. Electronic mail: daniel.grischkowsky@okstate.edu.
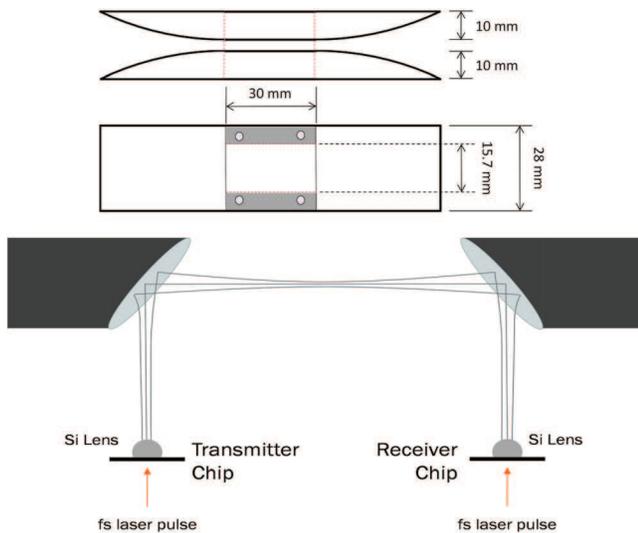
FIG. 1. Top: Dimensions of the CYLWG. Top figure is the side view, and the bottom figure is the top-down view of a single plate showing the milled out 28×30 mm region for the plate of the PPWG. The dashed 15.7×30 mm region defines the open area of the waveguide. The centered hole pattern is 21 mm $\times 20$ mm, and the total length of the CYLWG is 111.5 mm. The spacers are shown in grey with precisely located punched holes for passage of the connecting screws. Bottom: Standard THz-TDS system.

plate spacings (gaps) that were approximately doubled in size, 12.5, 25, 50, 100, and 200 μm. Free-space THz pulses were also measured between the measurements for the different gap sizes by removing the waveguide from the system. FFTs of the transmitted pulses gave the amplitude spectra, which were used for the analysis.

The transmission measurements through the aluminum waveguide showed that the CYLWGs performed as well as the silicon-lens coupled PPWGs. Fig. 2 shows the transmitted pulses (top) and the spectral data (bottom) for free-space

and the waveguide with different plate spacings. Fig. 3 shows the transmission measurements through the aluminum CYLWG, and Fig. 4 for the copper CYLWG.

In Figs. 2–4, the decrease in transmission with smaller gaps is clearly seen. As shown in Fig. 2 for a 200 μm gap, the transmission through the waveguide at 1 THz is 22%. However, removal of absorption effects shows the coupling to be 28%, comparable to that of silicon lenses.[9] Analysis to be presented later will show that this coupling is constant for all gap sizes, and that the reduced transmission occurs due to absorption in the skin-depth layer of the metal.

IV. THEORETICAL ANALYSIS

The reflectionless transmission[11] of THz pulses through the CYLWG is initially assumed to be a function of the gap size and the absorption at each gap designated by g, as given below

$$T_g = C_g(\omega)e^{-\alpha_g(\omega)L}, \tag{1}$$

where T_g is the amplitude transmission, C_g is the (initially assumed gap dependent) frequency dependent coupling into and out of the TEM mode of the CYLWG, α_g is the TEM-mode, gap-dependent absorption, and L is the 30 mm length of the flat parallel-plate region of the CYLWG. The amplitude spectrum $A_{t,g}(\omega)$ transmitted through the waveguide is given by the free-space input pulse spectrum, $A_o(\omega)$, multiplied by the CYLWG transmission T_g

$$A_{t,g}(\omega) = A_o(\omega)T_g = A_o(\omega)C_g(\omega)e^{-\alpha_g(\omega)L}. \tag{2}$$

$A_{t,g}$ can be seen in Figs. 2–4. The comparison with free-space transmission for the aluminum CYLWG is also shown in Fig. 2. To show that the waveguide coupling is independent of gap and that the changes in transmission with gap are only due to absorption effects, we first examine the relative coupling of the waveguide with respect to the largest gap
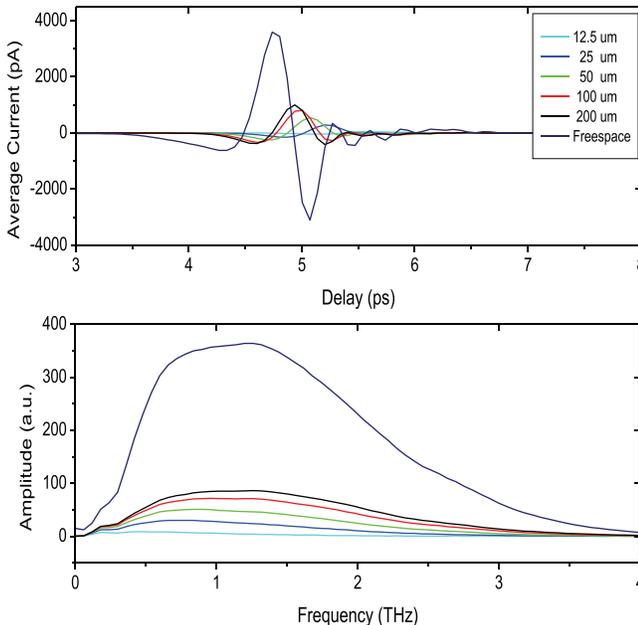

FIG. 2. Top: Transmitted THz pulses through free-space and the aluminum CYLWG with various gap sizes and through free-space. The measured pulse durations have been cut to show only from 3 to 8 ps for clarity. Bottom: Corresponding amplitude spectra.
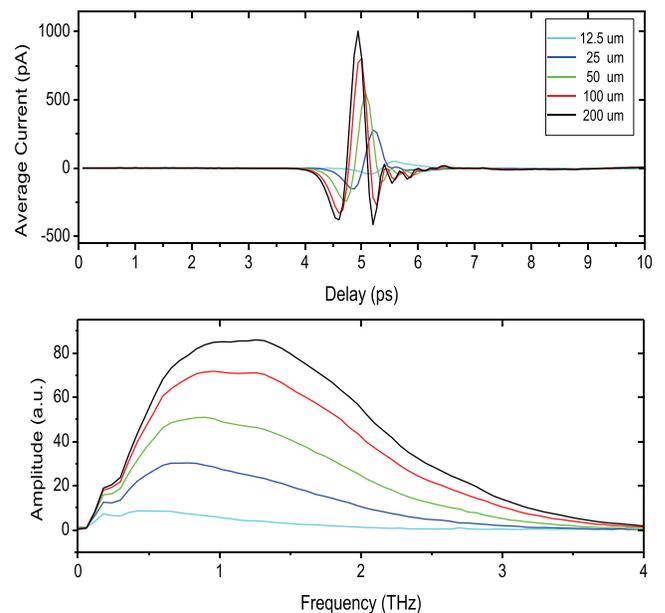

FIG. 3. Top: Transmitted THz pulses through the aluminum CYLWG. Bottom: Corresponding amplitude spectra.

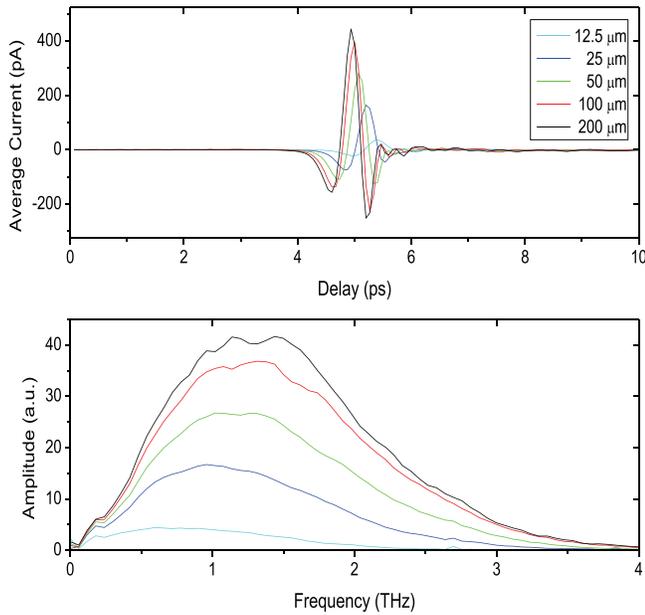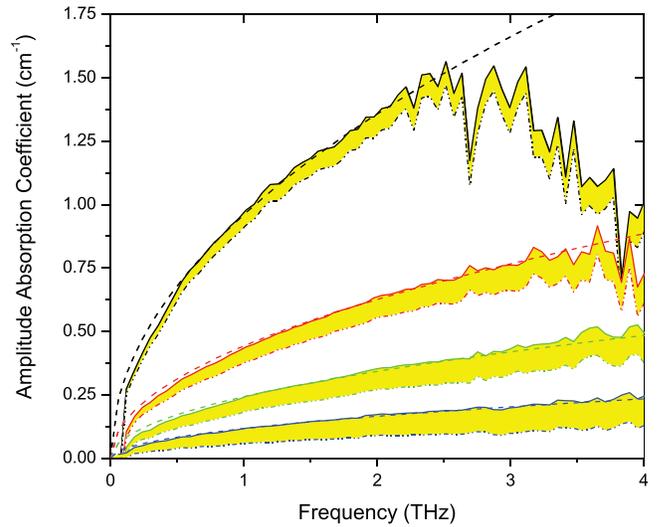FIG. 4. Top: Transmitted THz pulses through the copper CYLWG. Bottom: Corresponding amplitude spectra.

FIG. 5. The measured amplitude absorption coefficients (ACs) for an aluminum CYLWG with different gaps. The dashed lines are the theoretical fits using the strength parameter S from Table I and the $\sqrt{f}$ dependence. From the top curve, $g = 11.9\,\mu m$, $g = 22.5\,\mu m$, $g = 50\,\mu m$ and to the bottom curve $g = 100\,\mu m$. The upper boundary is AC for each high-lighted curve, and the lower boundary is the relative amplitude absorption coefficient (RAC), relative to the $200\,\mu m$ gap measurement. RAC = RA/L, where L is the waveguide length of 3 cm and RA = $-\ln\,[A_{tg}(\omega)/A_{t200}(\omega)]$ from Eq. (4). As shown by Eqs. (8) and (9), AC = RAC + AC ($g = 200\,\mu m$), for which RAC ($g = 100\,\mu m$) = AC ($g = 200\,\mu m$). The S/N ratio and the dynamic range of the receiver limits the accuracy of the $g = 11.9\,\mu m$ measurement to 2.0 THz and the $g = 22.5\,\mu m$ measurement to 3.0 THz. The sharp fall-offs beyond these limits are instrumental limitations.

size of $200\,\mu m$, rather than to free-space. This ratio will demonstrate that the amplitude coupling C_g is independent of gap. These relative transmission measurements are given by

$$\frac{A_{t,g}(\omega)}{A_{t,200}(\omega)} = \frac{C_g(\omega)}{C_{200}(\omega)}\,e^{-(\alpha_g - \alpha_{200})L}. \tag{3}$$

The relative absorbance RA $= (\alpha_g - \alpha_{200})L$ for each gap is obtained from Eq. (3) as

$$RA = (\alpha_g - \alpha_{200})\,L = \ln\frac{C_g(\omega)}{C_{200}(\omega)} - \ln\frac{A_{t,g}(\omega)}{A_{t,200}(\omega)}. \tag{4}$$

Dividing RA by the 3 cm length L of the parallel-plate region gives the relative absorption coefficient (RCA) of the waveguide, shown in Fig. 5 as the lower dashed-dotted-dotted lines for the aluminum CYLWG, and also in Fig. 6 for the copper CYLWG.

The theoretical absorption coefficient for the parallel plate metal waveguide is well known and is given in textbooks and handbooks by[14,15]

$$\alpha_0 = R/(\eta_0 g)\,(m)^{-1}. \tag{5}$$

$$R = 10.88 \times 10^{-3}[10^7/(\sigma\lambda_0)]^{0.5}\,\Omega, \tag{6}$$

where R is the metal impedance, η_0 is the free-space wave impedance of 377 Ω, g is the gap size, and σ is the conductivity of the metal.

The dependence on frequency and conductivity becomes clear when the two equations are combined to form the simpler mathematical expression in Eq. (7), where the frequency f is expressed in units of THz, or 10^{12}, σ is in terms of 10^7 $(\Omega\,m)^{-1}$, and η_0 is replaced by 377 Ω

$$\alpha_0 = 1.6662 \times 10^{-3}\left[\frac{f}{\sigma}\right]^{0.5}\left(\frac{1}{g}\right). \tag{7}$$

From this equation, it is now explicitly apparent that the absorption has both a $\sqrt{f}$ dependence and an inverse proportionality to g. We use this simple dependence to test the accuracy of our results from Figs. 5 and 6 and to show that the
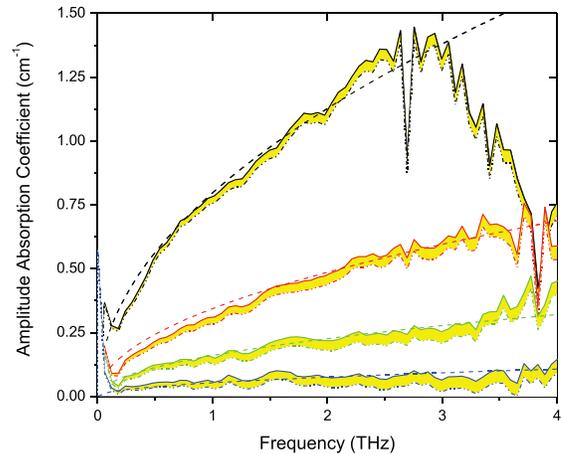

FIG. 6. The measured ACs for a copper CYLWG with different gaps. The dashed lines are the theoretical fits using the strength parameter S from Table I and the $\sqrt{f}$ dependence. From the top curve, $g = 10\,\mu m$, $g = 23.4\,\mu m$, $g = 50\,\mu m$, and bottom curve $g = 100\,\mu m$. The upper boundary is AC for each high-lighted curve, and the lower boundary is the RAC, relative to the $200\,\mu m$ gap measurement. RAC = RA/L, where L is the waveguide length of 3 cm and RA = $-\ln\,[A_{tg}(\omega)/A_{t200}(\omega)]$ from Eq. (4). As shown by Eqs. (8) and (9), AC = RAC + AC ($g = 200\,\mu m$), for which RAC ($g = 100\,\mu m$) = AC ($g = 200\,\mu m$). The S/N ratio and the dynamic range of the receiver limits the accuracy of the $g = 10.0\,\mu m$ measurement to 2.5 THz and the $g = 23.4\,\mu m$ and $g = 50\,\mu m$ measurements to 3.5 THz. The sharp fall-offs beyond these limits are instrumental limitations.

coupling is independent of gap size. The observations shown in Figs. 5 and 6 do indeed display a good $\sqrt{f}$ dependence fit (dashed lines) and the absorption is almost inversely proportional to g, thereby confirming that $\ln \frac{C_g(\omega)}{C_{200}(\omega)} = 0$.

This analysis assumes that there is no reflection at the entrance to the PPWG at the end of the coupling horn antenna. This assumption is based on the observed absence of a midpoint reflection from an adiabatically compressed PPWG, 63.5 mm long with entrance and exit gaps of 103 μm, and with a compressed mid-point gap of only 8 μm.[11] For this case, no mid-point amplitude reflection (above 1% of the transmitted signal) was observed. Consequently, this adiabatic no-reflection assumption predicts that there is no effective limit to the minimum gap size. For perfect conductors, as the CYLWG's gap becomes smaller and smaller, the CYLWG would continue to provide adiabatic compression for THz radiation, limited only by the flatness of the plates.

However, for air-spaced normal metal plates, the minimum gap is determined by the general condition that the absorption coefficient α_{gLimit}, due to the waveguide loss, must be much less than $1/\lambda$, where λ is the guided wavelength.[17] When this limit is approached, the approximations made for the propagating wave equation solutions are no longer valid and the lumped element regime of electronics is approached. For our aluminum CYLWG measurement shown in Fig. 5 and using the theoretical fit S parameter for g = 11.9 μm of Table I, if we set $\alpha_o = \alpha_{gLimit} = 1/\lambda_o$, and solve for g at the frequencies 0.5 (600 μm), 1.0 (300 μm) and 2 (150 μm) THz, we obtain the limiting gaps g of 0.48 μm, 0.34 μm, and 0.24 μm, respectively. It is reasonable to assume that an absorption length (1/e for amplitude) of 10 wavelengths would still give good waveguide propagation, which corresponds to the limiting operational gaps g of 4.8 μm, 3.4 μm, and 2.4 μm, for 0.5, 1, and 2 THz, respectively. These results are also important to understand the fundamental sensitivity limits of waveguide THz-TDS.[2–4]

For our case, the wave equation solutions are still valid, and Eq. (3) can now be rewritten with $C_g(\omega)$ now simplified to $C(\omega)$

$$\frac{A_{t,g}(\omega)}{A_{t,zero\ \alpha}(\omega)} = \frac{C(\omega)}{C(\omega)} e^{-\alpha_g(\omega)L}. \tag{8}$$

The measurements can now be normalized to the non-absorption waveguide, by noting that the g dependence shows $\alpha_{100} = 2\,\alpha_{200}$

$$\frac{A_{t,100}(\omega)}{A_{t,200}(\omega)} = e^{-(\alpha_{100}-\alpha_{200})L} = e^{-(\alpha_{200})L}. \tag{9}$$

TABLE I. Measured strength parameters S of the different gaps, given in units of 1/cm. To obtain the absorption coefficient, multiply by $\sqrt{f}$ in THz. Note that S = α at 1 THz.

Aluminum	11.9 μm	22.5 μm	50 μm	100 μm
S	0.95	0.445	0.25	0.120
Copper	10 μm	23.4 μm	50 μm	100 μm
S	0.78	0.33	0.155	0.054

Consequently, the 200 μm absorbance can be added to all the curves to obtain the actual absorption coefficients, as shown by the solid lines in Figs. 5 and 6, marking the top of the high-lighted regions indicating the addition.

V. RESULTS AND DISCUSSION

As stated earlier, the measurements shown in Figs. 5 and 6 exhibit a good fit to the $\sqrt{f}$ dependence (dashed lines). These calculated $\sqrt{f}$ fits have been multiplied by the strength parameter S, given in Table I, adjusted to achieve the best fit to the total measured absorption, for which the 200 μm absorption has been added to the relative absorption (dashed-dotted-dotted) lines. These accurate fits verify that our waveguides have constant coupling over the range of gap sizes, in contrast to the gap dependent overlap integral description of the quasi-optical coupling of the silicon lenses to the PPWG.[16]

The inverse proportionality to gap size is also evident, as shown in Table I, for which the absorption coefficient for each gap is given by the strength parameter S, in units of 1/cm, multiplied by $\sqrt{f}$, where f is the frequency in THz. Here, the measured thicknesses of the metal spacers used to create the gaps are given. The deviations from a strict 1/g dependence is considered to be due to not having flat surfaces over the waveguide plates, for which smoothly varying surface features of the order of microns were present.

By substituting into Eq. (7), the measured absorption value, the specified frequency, and the gap size, the conductivity factors of the waveguide metals were determined. For aluminum, the measured conductivity factor was 1.9, and for copper, 3.5 was obtained. The handbook conductivity factors for aluminum and copper are 3.72 and 5.80, respectively.[15] For each metal, the measured conductivity in the THz skin depth layer is significantly less than the bulk value. As seen in previous publications,[10] this reduction in conductivity is expected and can be attributed to carrier scattering due to lattice defects in the layer.

VI. CONCLUSION

The loss free coupling of 28% of the reflection-free CYLWG is comparable to the silicon-lens based method of coupling with 32% for the best case.[9] The major advantage is that the frequency dependent coupling of the easily assembled CYLWG is quite reproducible and is independent of the waveguide gap. Given flat smooth surfaces on the waveguide plates, the gaps could be reduced to 5 μm and still retain the same coupling, which would be impossible to do with the gap dependent coupling of the silicon-lens coupled waveguides. The reflection free CYLWG waveguides are also significantly easier to use, since there are no additional lenses or other parts that need to be precisely aligned.

ACKNOWLEDGMENTS

[1]R. Mendis and D. Grischkowsky, "Undistorted guided wave propagation of sub-picosecond THz pulses," Opt. Lett. **26**, 846–848 (2001).

[2]J. Zhang and D. Grischkowsky, "Waveguide THz time-domain spectroscopy of nm water layers," Opt. Lett. **19**, 1617–1619 (2004).

[3]J. S. Melinger, N. Laman, S. Sree Harsha, S. Cheng, and D. Grischkowsky, "High-resolution waveguide terahertz spectroscopy of partially oriented organic polycrystalline films," J. Phys. Chem. **111A**, 10977 (2007).

[4]N. Laman, S. Sree Harsha, D. Grischkowsky, and J. S. Melinger, "7 GHz resolution waveguide THz spectroscopy of explosives related solids showing new features," Opt. Express **16**, 4049–4105 (2008).

[5]C. Rau, G. Torosyan, R. Beigang, and Kh. Nerkararyan, "Prism coupled terahertz waveguide sensor," Appl. Phys. Lett. **86**, 211119 (2005).

[6]M. Theuer, R. Beigang, and D. Grischkowsky, "Highly sensitive terahertz measurement of layer thickness using a two-cylinder waveguide sensor," Appl. Phys. Lett. **97**, 071106 (2010).

[7]M. M. Awad and R. A. Cheville, "Transmission terahertz waveguide-based imaging below the diffraction limit," Appl. Phys. Lett. **86**(22), 221107–221107-3 (2005).

[8]A. Bingham, Y. Zhao and D. Grischkowsky, "THz parallel plate photonic waveguides," Appl. Phys. Lett. **87**, 051101 (2005).

[9]Y. Zhao and D. Grischkowsky, "2-D THz metallic photonic crystals in parallel plate waveguides," IEEE Trans. Microwave Theory Techn. **55**, 656–663 (2007).

[10]N. Laman and D. Grischkowsky, "Reduced conductivity in the terahertz skin-depth layer of metals," Appl. Phys. Lett. **90**, 122115 (2007).

[11]J. Zhang and D. Grischkowsky, "Adiabatic compression of parallel-plate metal waveguides for sensitivity enhancement of waveguide THz time-domain spectroscopy (THz-TDS)," Appl. Phys. Lett. **86**, 061109 (2005).

[12]M. Theuer, A. J. Shutler, S. Sree Harsha, R. Beigang, and D. Grischkowsky, "Terahertz two-cylinder waveguide coupler for transverse-magnetic and transverse-electric mode operation," Appl. Phys. Lett. **98**, 071108 (2011).

[13]S.-H. Kim, E. S. Lee, Y. B. Ji, and T.-I. Jeon, "Improvement of THz coupling using a tapered parallel-plate waveguide," Opt. Express **18**, 1289–1295 (2010).

[14]N. Marcuvitz, *Waveguide Handbook* (Peregrinus, London, 1993), Chap. 2, p. 64.

[15]S. Ramo, J. R. Whinnery, and T. van-Duzer, *Fields and Waves in Communications Electronics*, 3rd ed. (John Wiley and Sons, Inc., New York, 1994), Chap. 8.5, p. 408.

[16]J. C. G. Lesurf, "Beam coupling, lenses and mirrors," in *Millimetre-Wave Optics, Devices and Systems* (Adam Hilger, Bristol, 1990), pp. 11–28.

[17]W. J. Gallagher, C.-C. Chi, I. N. Duling III, D. Grischkowsky, N. J. Halas, M. B. Ketchen, and A. W. Kleinsasser, "Subpicosecond optoelectronic study of resistive and superconductive transmission lines," Appl. Phys. Lett. **50**, 350–352 (1987).